Reproducibility by Climate Models of Cloud Radiative Forcing Associated with Tropical Convection

HIROKI ICHIKAWA

*Department of Earth and Environmental Sciences, Graduate School of Environmental Studies,
Nagoya University, Nagoya, Japan*

HIROHIKO MASUNAGA

Hydrospheric Atmospheric Research Center, Nagoya University, Nagoya, Japan

YOKO TSUSHIMA

Met Office Hadley Centre, Exeter, United Kingdom

HIROSHI KANZAWA

*Department of Earth and Environmental Sciences, Graduate School of Environmental Studies,
Nagoya University, Nagoya, Japan*

ABSTRACT

In this study, cloud radiative forcing (CRF) associated with convective activity over tropical oceans is analyzed for monthly mean data from twentieth-century simulations of 18 climate models participating in phase 3 of the Coupled Model Intercomparison Project (CMIP3) in comparison with observational and reanalysis data. The analysis is focused on the warm oceanic regions with sea surface temperatures (SSTs) above 27°C to exclude the regions with cold SSTs typically covered by low stratus clouds. CRF is evaluated for different regimes sorted by pressure-coordinated vertical motion at 500 hPa ($\omega 500$) as an index of large-scale circulation. The warm oceanic regions cover the regime of vertical motion ranging from strong ascent to weak descent. The most notable feature found in this study is a systematic underestimation by most models of the ratio of longwave cloud radiative forcing (LWCRF) to shortwave cloud radiative forcing (SWCRF) over the weak vertical motion regime defined as $-10 < \omega 500 < 20$ hPa day^{-1}. The underestimation of the ratio corresponds to the underestimation of LWCRF and the overestimation of SWCRF. Clouds in models seem to be lower in the amount of high clouds but more reflective than those in the observations in this regime.

In the weak vertical motion regime, the lower free troposphere is dry. In the large-scale environment condition, the reproducibility of LWCRF is high in models adopting the scheme where the relative humidity–based suppression for deep convection occurrence is implemented. Models adopting the Zhang and McFarlane scheme show good performance without such a suppression mechanism.

1. Introduction

The radiative effect of clouds, often called cloud radiative forcing (CRF), associated with convective activity largely controls the radiative balance–imbalance at the top of the atmosphere (TOA) over the tropics through the horizontal extension of high clouds that accompany deep convection (Ramanathan and Collins 1991; Lindzen et al. 2001; Hartmann et al. 2001). The response of CRF associated with convective activity to an imposed climate perturbation is thus fundamental for our understanding of climate change, but shows no consistency in either sign or magnitude among different climate models in climate perturbation experiments (Bony et al. 2004; Wyant et al. 2006; Williams and Tselioudis 2007; Williams and Webb 2009). A detailed evaluation

Corresponding author address: Hiroki Ichikawa, Dept. of Earth and Environmental Sciences, Graduate School of Environmental Studies, Nagoya University, Furo-cho, Chikusa-ku, Nagoya 464-8601, Japan.
E-mail: ichikawa@hyarc.nagoya-u.ac.jp

of CRF associated with convective activity is warranted to provide physical insights into particular biases of the models in the CRF response.

The model reproducibility of CRF associated with convective activity depends on how the model deals with moist convection and its associated cloud properties. Previous studies evaluated different elements of clouds associated with convective activity in conjunction with dynamic and thermodynamic environments in models. Ichikawa et al. (2009) showed that the horizontal spread of high clouds around the center of upper-tropospheric divergence is underestimated over the large-scale ascending branch in models. Su et al. (2006) showed that the sensitivity of the cloud ice amount to sea surface temperature (SST) is underestimated in models and largely diverse among models. These biases would cause biases in the CRF.

Observational evidence has shown that, in the tropics, the longwave cloud radiative forcing (LWCRF) and shortwave cloud radiative forcing (SWCRF) are both strong and nearly cancel each other over the region where deep convection is active (Ramanathan 1989; Kiehl and Ramanathan 1990; Kiehl 1994; Hartmann et al. 2001). Recently, Yuan et al. (2008, hereafter Y08) reexamined the observed relationship between LWCRF and SWCRF in the tropics with consideration of the effects of the large-scale circulation. They revealed that, over warm oceanic regions with SST above 28°C, the two components of CRF nearly cancel each other regardless of the large-scale environment.

This study evaluates CRF associated with convective activity over tropical oceans in coupled atmosphere–ocean general circulation models (AOGCMs), considering the effects of the dynamic and thermodynamic environments. The area domain analyzed in this study is warm oceanic regions where shallow to deep convection develops in response to large-scale circulation in the troposphere and/or in conjunction with high moist static energy in the lower troposphere. First, we analyze the reproducibility of CRF for different regimes of large-scale circulation in climate models. The main focus of the analysis is on evaluating the relationship of the balance between LWCRF and SWCRF with large-scale circulation that was revealed observationally by Y08. We find a bias in the balance common to the models for particular regimes of large-scale circulation, and then devote our efforts to unraveling the physical causes for this common bias. This study employs a wide range of models with different types of cumulus parameterization schemes and large-scale condensation schemes, so that we can undertake a systematic intercomparison of the parameterization schemes among the models. Such an intercomparison

may provide useful information helpful for improving the model physics.

Section 2 outlines the observational and reanalysis data and model simulations used in this study. Section 3 describes a method for the analysis. Section 4 presents the results on the reproducibility of CRF associated with convective activity in the models as described above. Section 5 is devoted to a discussion on the result. Section 6 presents our concluding remarks.

2. Data

a. Observational and reanalysis data

The data used to evaluate the model outputs include both observational and reanalysis datasets. The Earth Radiation Budget Experiment (ERBE) S-9 data (Barkstrom1984; Barkstrom and Smith 1986) are used to calculate CRF. The data contain monthly mean values of the reflected shortwave and emitted longwave fluxes at the TOA obtained from broadband scanner measurements. The International Satellite Cloud Climatology Project (ISCCP) D2 visible–infrared (VIS–IR) cloud data (Rossow and Schiffer 1999) are used for cloud amount, cloud-top pressure, and cloud water path. The 40-yr European Centre for Medium-Range Weather Forecasts (ECMWF) Re-Analysis (ERA-40) dataset (Uppala et al. 2005) is used for the atmospheric variables. Pressure-coordinated vertical velocity at 500 hPa, denoted by $\omega 500$, is used as an index of the large-scale circulation field. The Hadley Centre Global Sea Ice and Sea Surface Temperature (HadISST) analyses (Rayner et al. 2003) are used for SST. For a comparison with a model output, all these data are interpolated onto the common $2.5° \times 2.5°$ grid, the same coordinate system as in ERA-40, using the method of Kosaka et al. (2009). Monthly averages for 5 yr and 1 month during February 1985–February 1990 are used for the analysis. The period of the analysis is limited by the observational period of ERBE.

b. Climate models

1) OVERVIEW

This study uses outputs from the twentieth-century climate simulations conducted with the 18 AOGCMs listed in Table 1. These models were included in the Fourth Assessment Report (AR4) of the Intergovernmental Panel on Climate Change (IPCC; Solomon et al. 2007), and their data were submitted to the Program for Climate Model Diagnosis and Intercomparison (PCMDI). These archived data constitute phase 3 of the World Climate Research Programme's (WCRP) Coupled Model Intercomparison Project (CMIP3).

TABLE 1. Descriptions of the 18 coupled AOGCMs analyzed in this study (more information available online at http://www-pcmdi.llnl.gov/.)

Modeling group	Model (label in this paper)	Atmospheric resolution (lat × lon)	Cumulus parameterization scheme/modification (label in this paper)	LSC* parameterization scheme; coupling with cumulus parameterization scheme?
National Center for Atmospheric Research (NCAR)	Community Climate System Model, version 3 (CCSM3)	1.4° × 1.4°	Zhang and McFarlane (1995) (ZM)	Zhang et al. (2003); yes
Canadian Centre for Climate Modeling and Analysis (CCCma)	CCCma Coupled General Circulation Model, version 3.1 (CGCM-T47)	2.8° × 2.8°	Zhang and McFarlane (1995) (ZM)	McFarlane et al. (2005); no
	Same as above (CGCM-T63)	1.9° × 1.9°	Zhang and McFarlane (1995) (ZM)	McFarlane et al. (2005); no
Météo-France/Centre National de Recherches Météorologiques (CNRM)	CNRM Coupled Global Climate Model, version 3 (CNRM)	1.9° × 1.9°	Bougeault (1985) (MC)	Ricard and Royer (1993); no
Max Planck Institute for Meteorology (MPI)	ECHAM5/MPI Ocean Model (ECHAM5)	1.9° × 1.9°	Tiedtke (1989)/Nordeng (1994) (MC)	Lohmann and Roeckner (1996); yes
LASG/Institute of Atmospheric Physics	Flexible Global Ocean–Atmosphere–Land System Model gridpoint version 1.0 (FGOALS)	2.8° × 2.8°	Zhang and McFarlane (1995) (ZM)	Rasch and Kristjansson (1998); no
NOAA–Geophysical Fluid Dynamics Laboratory (GFDL)	GFDL Climate Model version 2.0 (GFDL2.0)	2.0° × 2.5°	Moorthi and Suarez (1992)/ Tokioka et al. (1988) (AS)	Tiedtke (1993); yes
	GFDL Climate Model version 2.1 (GFDL2.1)	2.0° × 2.5°	Moorthi and Suarez (1992)/ Tokioka et al. (1988) (AS)	Tiedtke (1993); yes
NASA Goddard Institute for Space Studies (GISS)	GISS Model E-H (GISS-EH)	4.0° × 5.0°	Del Genio and Yao (1993) (CBB)	Del Genio et al. (1996); yes
	GISS Model E-R (GISS-ER)	4.0° × 5.0°	Del Genio and Yao (1993) (CBB)	Del Genio et al. (1996); yes
Institute for Numerical Mathematics (INM)	INM Coupled Model, version 3.0 (INM)	4.0° × 5.0°	Betts (1986) (BE)	Diansky and Volodin (2002); no
Institute Pierre Simon Laplace (IPSL)	IPSL Coupled Model, version 4 (IPSL)	2.5° × 3.8°	Emanuel (1991)/ Grandpeix et al. (2004) (EM)	Bony and Emanuel (2001); yes
Center for Climate System Research, National Institute for Environmental Studies, and Frontier Research Center for Global Change	Model for Interdisciplinary Research on Climate 3.2, high-resolution version (MIROC-hi)	1.1° × 1.1°	Pan and Randall (1998)/ Emori et al. (2001) (AS)	Le Trent and Li (1991); no
	MIROC3.2, medium-resolution version (MIROC-me)	2.8° × 2.8°	Pan and Randall (1998)/ Emori et al. (2001) (AS)	Le Trent and Li (1991); no
Meteorological Research Institute (MRI)	MRI Coupled General Circulation Model, version 2.3.2 (MRI)	2.8° × 2.8°	Pan and Randall (1998) (AS)	Yukimoto et al. (2006); no
NCAR	Parallel Climate Model, version 1 (PCM1)	2.8° × 2.8°	Zhang and McFarlane (1995) (ZM)	Rasch and Kristjansson (1998); no
Hadley Centre for Climate Prediction and Research/Met Office	Third climate configuration of the Met Office Unified Model (HadCM3)	2.5° × 3.8°	Gregory and Rowntree (1990) (CBB)	Smith (1990); no
	Hadley Centre Global Environmental Model, version 1 (HadGEM1)	1.3° × 1.9°	Gregory and Rowntree (1990) (CBB)	Wilson and Ballard (1999); no

* LSC = large-scale condensation.

The twentieth-century simulations by the models are evaluated by using monthly mean outputs for the 20 yr during 1980–99 so that the data period covers that of the observations (February 1985–February 1990) and is long enough to evaluate the climatological features of the model reproducibility. All the variables are interpolated onto the common $2.5° \times 2.5°$ grid, the same as the observational and reanalysis datasets, using the method of Kosaka et al. (2009). Most models do not use the surface flux corrections, with four exceptions (CGCM-T47, CGCM-T63, INM, MRI; see Table 1 for model acronyms).

2) CUMULUS PARAMETERIZATION SCHEMES

Subgrid-scale cloudiness associated with tropical convection is largely controlled by a cumulus parameterization scheme adopted in each model. Several types of schemes are used as described below and in Table 1. More information on aspects of the cumulus parameterizations can be found in Dai (2006) and Lin (2007).

Some models adopt a scheme based on mass flux approaches with spectral cloud models similar to Arakawa and Schubert (1974). The scheme is hereafter named AS (GFDL2.0, GFDL2.1, MIROC-hi, MIROC-me, MRI). The convective trigger–closure of this scheme links basically to the convective available potential energy (CAPE). Some models adopting this scheme incorporate the threshold of relative humidity proposed by Emori et al. (2001) (MIROC-hi, MIROC-me) to trigger the convection or, alternately, the threshold of the entrainment rate by Tokioka et al. (1988) (GFDL2.0, GFDL2.1). The incorporation of these thresholds acts to relate an accumulation of moisture to the convection occurrence in the model simulations.

Two types of schemes adopted in some models are based on the bulk cloud model, where an ensemble of clouds is approximated by one single cloud. For one type, the convective trigger–closure is based on the cloud-base buoyancy proposed by Gregory and Rowntree (1990) and Del Genio and Yao (1993). The scheme is hereafter named CBB (GISS-EH, GISS-ER, HadCM3, HadGEM1). For the other type of scheme, the convective trigger–closure is based on the moisture convergence concept originally proposed by Kuo (1965). The scheme is hereafter named MC (CRNM, ECHAM5).

Some models adopt the scheme proposed by Zhang and McFarlane (1995), which is based on the spectral rising plume concept as in the AS scheme but assumes a constant spectral distribution in the cloud-base mass flux. The scheme is hereafter named ZM (CCSM3, CGCM-T47, CGCM-T63, FGOALS, PCM1). The convective trigger–closure of this scheme links basically to CAPE. This scheme is primarily designed for deep rather than shallow cumulus convection. The top of the shallowest plume among the spectral rising plumes is higher than the height where the moist static energy exhibits its minimum in its vertical profile at each grid point. In the tropics, the minimum typically appears in the middle troposphere in association with a deep conditionally unstable layer.

A model (INM) adopts the lagged convective adjustment scheme proposed by Betts (1986). This scheme is hereafter named BE. The BE scheme adjusts the thermodynamic field toward a reference thermodynamic field for shallow and deep convection. For deep convection adjustment, the total enthalpy between the cloud base and cloud top is needed to be conserved. Because of the enthalpy constraint, the deep convection adjustment is not activated when dry warm layers exist in the model atmosphere (see Baldwin et al. 2002 for details).

A model (IPSL) adopts the scheme proposed by Emanuel (1991) where the collective effects of the various subparcels in the cloud are represented by a buoyancy sorting approach. This scheme is hereafter named EM. To achieve the inhomogeneous and episodic occurrence of mixing of the environmental air into a cloud, a finite number of subparcels that contain different fractions of environmental and cloudy air are assumed using a probability distribution for the mixing fraction. The IPSL model adopts a probability distribution that makes the convection sensitive to the relative humidity profiles in the free troposphere, as proposed by Grandpeix et al. (2004). The probability distribution acts to suppress deep convection when the free troposphere is under dry conditions in the model simulations.

3) COUPLING BETWEEN THE CUMULUS PARAMETERIZATION AND LARGE-SCALE CONDENSATION PARAMETERIZATION SCHEMES

Representations of cirrus clouds detrained from deep convection in models may be classified into two distinct groups as follows. In some models, the cumulus parameterization scheme and the large-scale condensation scheme are allowed to interact. More specifically, detrained cloud water from cumulus convection is made available for the calculation of stratiform cloud condensates. This type of model is hereafter named coupled (CCSM3, ECHAM5, GFDL2.0, GFDL2.1, GISS-EH, GISS-ER, IPSL). In other models, stratiform cloud condensates are calculated only from large-scale variables without being related directly to the subgrid-scale convective activity. This type of model is hereafter named decoupled (CCCMA-T47, CCCMA-T63, CNRM, FGOALS, INM, MIROC-hi, MIROC-me, MRI, PCM1, HadCM3, HadGEM1).
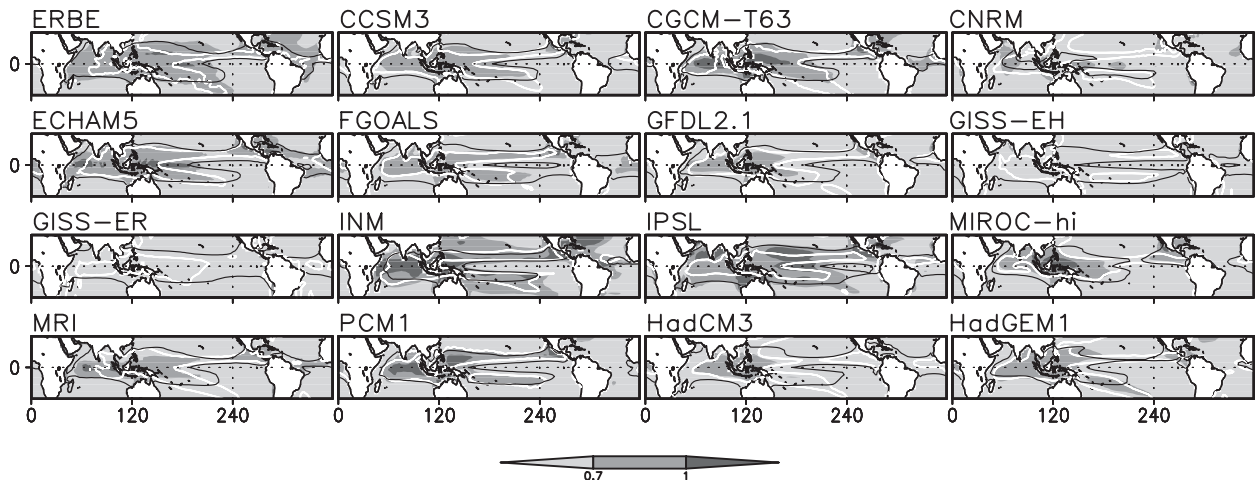
FIG. 1. Horizontal distributions of annual mean R (in grayscale) for the ERBE observations and the 15 models. Contours of $\omega 500$ at -15 hPa day^{-1} (white solid line) and SST at 27°C (black solid line) are superposed. Three models of CGCM-T47, GFDL2.0, and MIROC-me are not shown because the horizontal patterns of these three models are similar to the other versions of the same models (i.e., CGCM-T63, GFDL2.1, and MIROC-hi).

3. Method

a. Calculation of the cloud radiative forcing

Climatological features of CRF associated with cloud types prevalent for different regimes of large-scale circulation are analyzed on a monthly mean basis. Following Charlock and Ramanathan (1985), CRF is calculated as

$$\text{LWCRF} \equiv \text{OLR}_{\text{cl}} - \text{OLR},$$

$$\text{SWCRF} \equiv \text{TRS}_{\text{cl}} - \text{TRS}, \quad \text{and}$$

$$\text{NetCRF} \equiv \text{LWCRF} + \text{SWCRF}.$$

Here, OLR and TRS refer to the outgoing longwave radiation and the total reflected solar radiation, respectively, at the TOA for all-sky conditions. Both OLR_{cl} and TRS_{cl} refer to the radiation for clear-sky conditions. Note that clouds have the effect of warming the atmosphere–surface system if their NetCRF is positive.

The analysis in this study includes a comparison of the magnitudes of LWCRF and SWCRF, as has been studied previously (e.g., Hartmann and Doelling 1991; Kiehl 1994; Cess et al. 2001). We analyzes the ratio of LWCRF to SWCRF calculated as

$$R \equiv -\frac{\text{LWCRF}}{\text{SWCRF}},$$

where R is a relative measure comparing the magnitudes of LWCRF and SWCRF. The quantity R equals one when LWCRF and SWCRF completely compensate each other to make NetCRF equal to zero. In this study, R is calculated from the climatologies of LWCRF and SWCRF, obtained as the mean value of the full period analyzed in this study (ERBE observations, February 1985–February 1990; models, 1980–99), for each grid point (Fig. 1) or each regime of large-scale circulation (Fig. 3d).

b. Calculation of high-cloud amount

This study analyzes the model reproducibility of the cloud amount in the ISCCP observations. Considering the fact that subgrid-scale clouds in models are expressed by a prescribed parameterization, it is difficult to evaluate clouds in models exactly. Nevertheless, evaluation of cloud amount would be necessary to provide physical insights into the model bias of CRF.

In section 5a, we compare high-cloud amounts in models with the ISCCP observations. Several objective methods for quantitatively characterizing the clouds in the models have been developed. The ISCCP simulator, which classifies the model's clouds into the same cloud types as in ISCCP using the model's radiation schemes, is useful for this characterization (e.g., Klein and Jakob 1999; Webb et al. 2001). However, the ISCCP simulator products are not available for the twentieth-century climate simulations in CMIP3 model outputs. This study adopts the maximum overlap assumption developed by Weare (2004) to calculate the high-cloud amount for models where the cloud amount is available for multiple vertical layers. High-cloud amount is assumed to be the largest value of the cloud fraction among all levels, with pressures between 440 and 50 hPa. The detection of high clouds based on this definition in the models closely follows the detection of high clouds in the ISCCP observations as seen from satellite.

In section 4b, we compare the total cloud amount in the CMIP3 model outputs with the ISCCP observations.

TABLE 2. Definition of regimes for $\omega500$ (hPa day^{-1}) in this study.

Strong ascent	Moderate ascent	Weak vertical motion	Moderate to strong descent
$\omega500 < -40$	$-40 < \omega500 < -10$	$-10 < \omega500 < 20$	$\omega500 > 20$

The total cloud amount in the models is defined as the cloud fraction for the whole atmosphere column as seen from the surface or the top of the atmosphere.

c. Analysis domain

This study analyzes the tropics (i.e., the range of latitude between 30°S and 30°N). In particular, this study is focused on oceanic regions with SSTs above 27°C to exclude the regions with cold SSTs typically dominated by low-level stratus clouds. Over the warm oceanic regions, LWCRF and SWCRF turn out to nearly cancel each other independently of different regimes of large-scale circulation in the ERBE observations (cf. Fig. 3d), as was revealed by Y08. We intensively evaluate the model reproducibility of the observations in section 4a. The near cancellation is not seen over the region with a cold sea surface because the impacts of low-level stratus clouds on SWCRF are much larger than are those on LWCRF (Y08).

4. Results

a. Analysis for the whole oceanic regions with warm SST

In this section, we analyze the model reproducibility of CRF over warm oceanic regions for the entirety of the tropics.

1) HORIZONTAL DISTRIBUTION OF R, $\omega500$, AND SST

First, we evaluate the general features of the CRF, large-scale circulation, and SST. Figure 1 shows the horizontal distributions of R (in grayscale) for the ERBE observations and models, superposed by $\omega500$ contoured at -15 hPa day^{-1} (white solid lines) and SST at 27°C (black solid lines). The horizontal distributions of $\omega500$ and SST for most models generally agree with ERA-40 and HadISST. The models reproduce well a wide area of ascent motion around the Maritime Continent surrounded by warm oceanic regions and a zonal band of ascent motion associated with the intertropical convergence zone (ITCZ) over the Pacific. This study focuses on the region with SSTs above 27°C, corresponding to regions enclosed by the black solid lines. Close examinations reveal that the area of the warm SST region varies among the models. Considerable differences between the ERBE observations and models, and among the models themselves, exist for the horizontal distribution of R. In the ERBE observations, R has nearly homogeneous values of about 0.8–0.9 within the warm SST region. In most models, within the warm SST region, R largely varies spatially (e.g., FGOALS, GFDL2.1, MIROC-hi, MRI, HadCM3) or is nearly homogeneous but underestimated (e.g., GISS-EH, GISS-ER).

2) RELATIONSHIP OF CRF WITH $\omega500$

It is well known that large-scale circulation largely controls the cloudiness and consequently CRF (Hartmann and Michelsen 1993; Bony et al. 1997; Williams et al. 2003). Thus, evaluating CRF for different regimes of large-scale circulation may be quite useful to unravel the
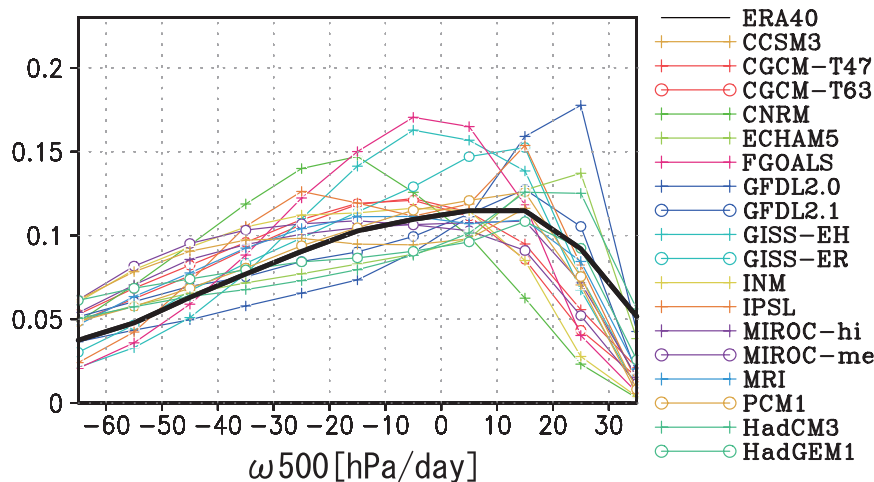
FIG. 2. PDF of $\omega500$ for each bin of 10 hPa day^{-1} width within the domain of SSTs above 27°C for ERA-40 (black solid line) and the 18 models (colored solid lines).
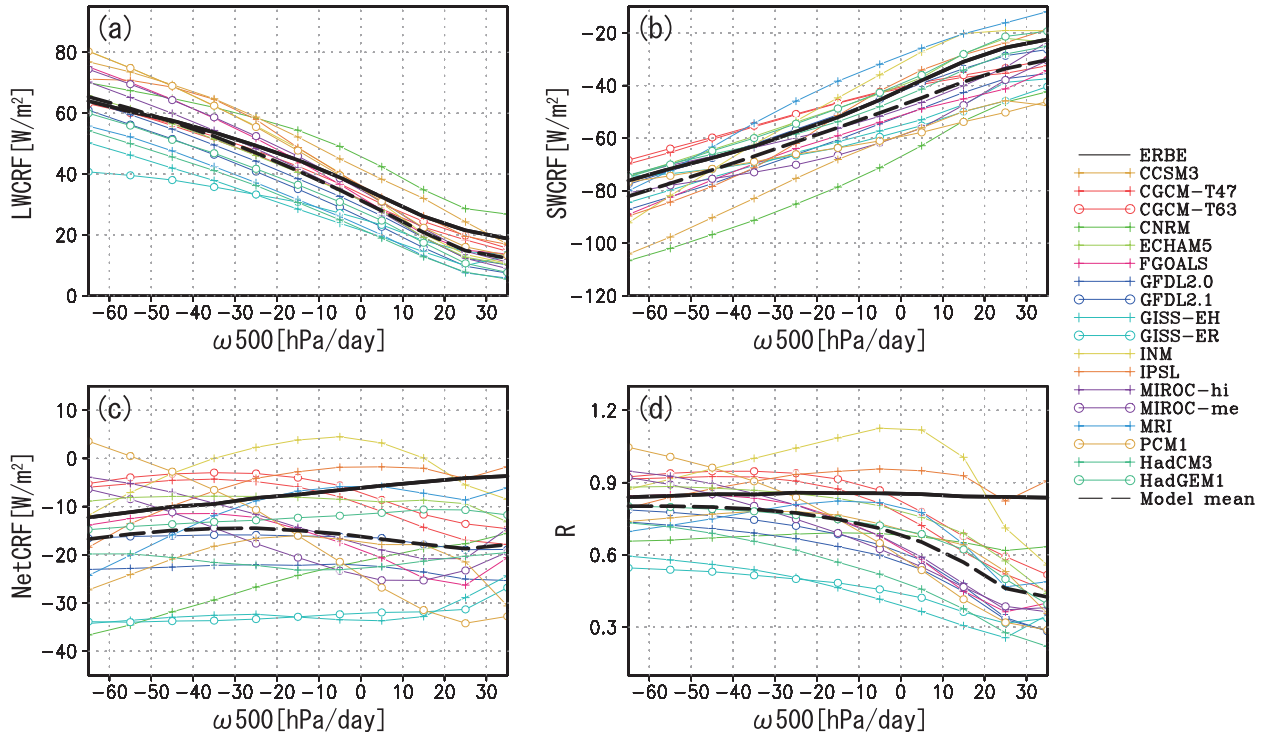
FIG. 3. Composites of (a) LWCRF, (b) SWCRF, (c) NetCRF, and (d) R as functions of $\omega 500$ within the domain of SSTs above 27°C for the ERBE observations (black solid line), the 18 models (colored solid lines), and the model mean for the models (black dashed line).

biases in the individual cloud types and the associated CRF in the models. We compute a composite of CRF for each regime of large-scale circulation sorted by bins of 10 hPa day^{-1} width in $\omega 500$. Table 2 shows the regime definitions in this study.

Figure 2 shows the probability density function (PDF) of $\omega 500$ in the domains of warm SSTs above 27°C for ERA-40 and the models. In ERA-40, the PDF exhibits at the descent, a peak of $\sim +10$ hPa day^{-1}, declining gradually to stronger ascents and sharply to stronger descents. The frequency of occurrence is high for the weak vertical motion regime of $-10 < \omega 500 < 20$ hPa day^{-1}, contributing to roughly 35% of the total in the domains of the warm SSTs. In most models, the PDF overall agrees with that in ERA-40. A closer examination reveals that the frequency of occurrence seems to be larger in the strong ascent regime while smaller in the moderate-to-strong descent regime in most models than in ERA-40.

Figure 3 shows the composites of (a) LWCRF, (b) SWCRF, (c) NetCRF, and (d) R as functions of $\omega 500$. LWCRF and SWCRF vary almost linearly with $\omega 500$ for both the ERBE observations and the models while they spread within a range of ~ 30 W m^{-2} at each $\omega 500$ in the models. The model biases of LWCRF are largely canceled out in the strong ascent regime, and the multimodel mean of LWCRF in the regime stays close to the ERBE

observations. In most models, LWCRF is underestimated in the weak vertical motion and moderate-to-strong descent regimes. SWCRF tends to be overestimated in many models; that is, it exceeds the observations in negative magnitude for all values of $\omega 500$.

The NetCRFs of the models are largely dispersed, suggesting a large uncertainty in the simulated CRF. In most models, NetCRF is underestimated for the weak vertical motion and moderate-to-strong descent regimes. For all values of $\omega 500$ in the ERBE observations, R is about 0.85. The model reproducibility of R worsens for the weak vertical motion and moderate-to-strong descent regimes where R is largely underestimated in most models. The model underestimation of R increases with increasing $\omega 500$. The underestimation of R is, by definition, ascribed to the underestimation of LWCRF and/or the overestimation of SWCRF.

b. Analysis for the weak vertical motion regime with warm SST

In this section, we analyze details of the model biases of LWCRF and SWCRF at $\omega 500 > -10$ hPa day^{-1}, where R is apparently underestimated in most models to unravel the physical causes of the biases. In particular, we focus on the weak vertical motion regime of $-10 < \omega 500 < 20$ hPa day^{-1}, where the frequency of occurrence is high
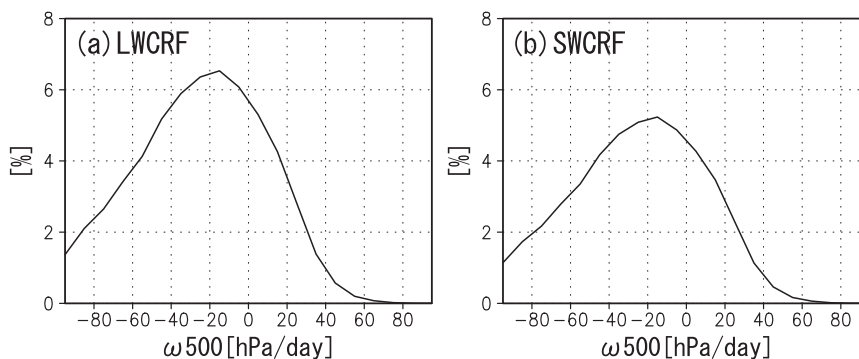
FIG. 4. Contribution of observed (a) LWCRF and (b) SWCRF for different $\omega500$s for the domain of SSTs above 27°C to those for the whole of the tropical oceans. The contribution is calculated as $(PDF_{\omega500}CRF_{\omega500})/CRF_{all}$, where $PDF_{\omega500}$ and $CRF_{\omega500}$ refer to the area normalized by the total area of the tropical oceans and the averaged value of CRF, respectively, for each bins of 10 hPa day^{-1} width of $\omega500$ over the domain of SSTs above 27°C. The quantity CRF_{all} refers to the mean value of CRF for all of the tropical oceans.

in ERA-40, as shown in Fig. 2. Figure 4 shows the contribution of LWCRF and SWCRF for different $\omega500$s for SSTs above 27°C to those for the whole of the tropical oceans in the ERBE observations. LWCRF and SWCRF for these regions contribute to 16% and 13% of those for the whole tropical oceans, respectively.

1) RELATIONSHIP BETWEEN LWCRF AND SWCRF

The model reproducibility of LWCRF and SWCRF is evaluated individually in the previous section but jointly in this section. We analyze the frequency occurrence of the two CRFs jointly, and compare the preferred combination of the two CRFs between the models and the ERBE observations. Figure 5 shows the joint PDF of LWCRF and SWCRF (in grayscale) for bins of 5 W m^{-2} width, calculated from data of each individual month at each grid point within the weak vertical motion regime. Contours of the observed PDF at 0.1%, 0.5%, and 2% (black solid contours) are superposed in each panel. Calculated from the climatologies of LWCRF and SWCRF for the weak vertical motion regime, R is also given in each panel. In the ERBE observations, the joint PDF distribution extends from the bottom left to the top right in the domain around the diagonal, indicating that LWCRF and SWCRF with roughly similar magnitude but opposite sign appear at each individual month. In the models, the joint PDF distribution extends from the bottom right to the top left similarly to the observation, but shows notable biases. In general, the joint PDF distribution tends to shift toward lower right compared to the ERBE observations for the models underestimating R, except CCSM3 and CNRM. It is noted that the frequency of occurrence in the range of large LWCRF and SWCRF in the top-right part of the panel is underestimated

for many models underestimating R. The underestimation of the frequency of occurrence is presumably associated with model bias of the cloudiness. Figure 6 shows the cloud-top pressure as a function of LWCRF and SWCRF. The domain of current interest near the top-right part is mainly dominated by high-top clouds with pressures lower than 440 hPa, indicating that large LWCRF and SWCRF are attributed mainly to high-top clouds. It follows that the models generally do not produce as many high clouds as are observed. We further discuss the model reproducibility of high clouds in section 5a.

2) RELATIONSHIP OF LWCRF WITH SST

We next analyze the possible factors for the systematic underestimation of LWCRF. The analysis is focused on the model reproducibility of the dependency of LWCRF on SST. Previous studies showed a drastic enhancement of deep convection and its associated high clouds, and the resultant increase in LWCRF over the regions with SSTs above ~27°C (e.g., Gadgil et al. 1984; Graham and Barnett 1987; Bony et al. 1997; Lau et al. 1997; Del Genio et al. 2005; Masunaga and Kummerow 2006). In the ERBE observations, as shown in Fig. 7, the increase in LWCRF with increasing SST from 26° to 29°C occurs not only in the strong and moderate ascent regimes but also in the weak vertical motion regime while LWCRF itself is smaller in the latter regime. The sensitivity of LWCRF to SST (i.e., gradient in Fig. 7) for the weak vertical motion regime is quite similar to that for other regimes for the range of SSTs above ~25°C. The decrease in LWCRF with increasing SST above 30°C is seen, as was revealed previously (Bony et al. 1997).

Figure 8 shows LWCRF as a function of SST for the weak vertical motion regime for the ERBE observations
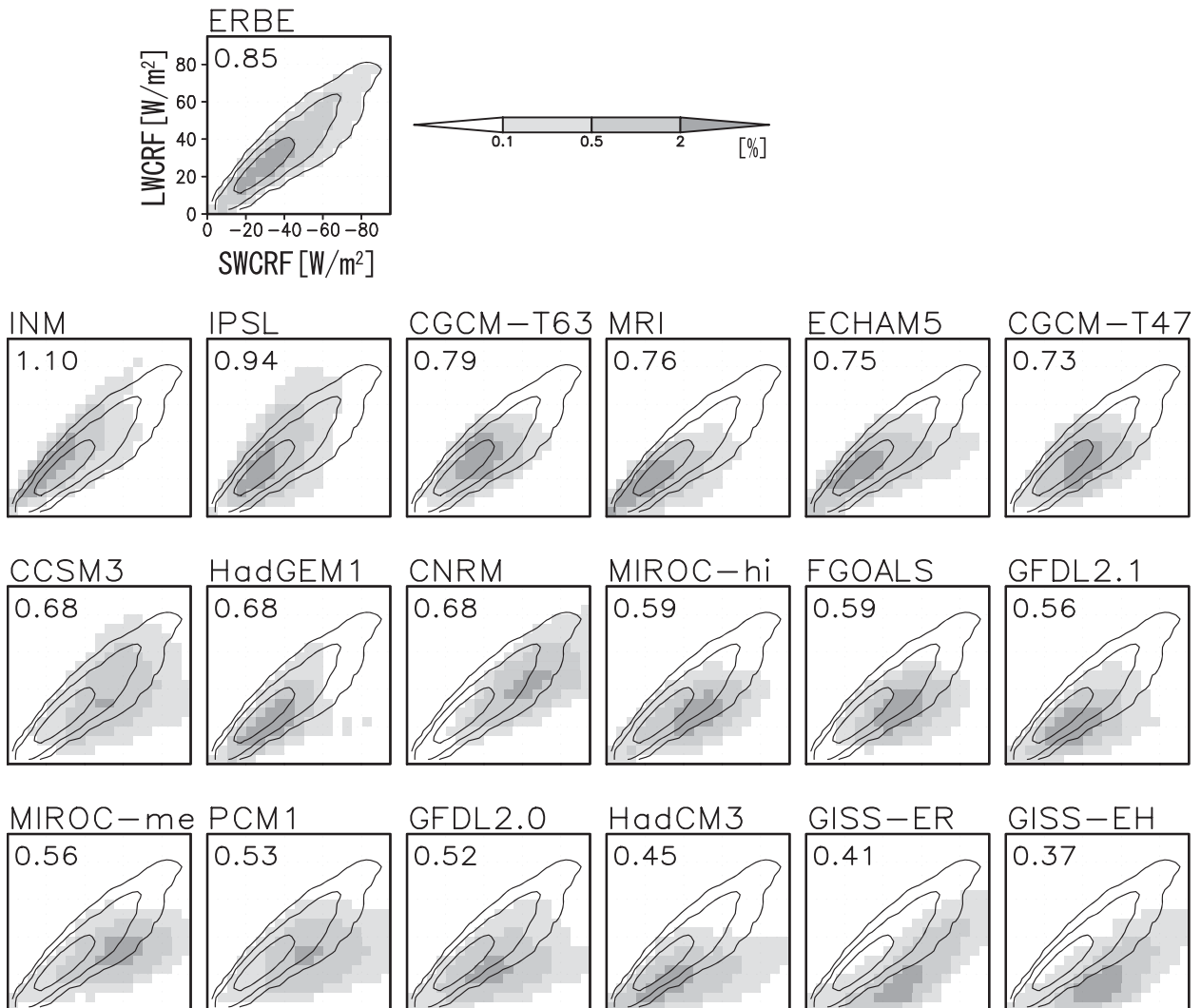
FIG. 5. Joint PDF of LWCRF and SWCRF (gray scale) over the weak vertical motion regime within the domain of SSTs above 27°C for the ERBE observations and the 18 models. Contours of PDF at 0.1%, 0.5%, and 2% for the observations (black solid lines) are superposed in each panel. The horizontal and vertical axes for the models are the same as those for the observations. Models are sorted by R, which is given in the top-left corner in each panel.

and models. The performance of the simulated LWCRF differs among models, particularly when SST is high. Most models fail to simulate the high sensitivity of LWCRF to SST from 26° to 29°C, although a few models successfully simulate it, and thus suffer from a significant underestimation of LWCRF over warm oceanic regions.

3) POTENTIAL RELEVANCE TO CUMULUS PARAMETERIZATION

The reproducibility of LWCRF is affected by that of deep convection, which is closely related to cumulus parameterization schemes adopted by models. Figure 9 shows the mean LWCRF for the weak vertical motion regime for the observations and models. The model reproducibility of LWCRF is assessed in terms of six types of cumulus parameterization schemes as described in section 2b. The reproducibility of LWCRF varies depending on the type of scheme adopted. In general, LWCRF is well reproduced in models adopting the BE, EM, and ZM schemes. On the other hand, LWCRF is systematically underestimated in models adopting the CBB scheme. The reproducibility of LWCRF differs among models adopting the AS scheme: the reproducibility tends to be good for the models adopting the threshold for triggering convection, and is particular high for the models adopting relative humidity–based suppression for their triggering convection.
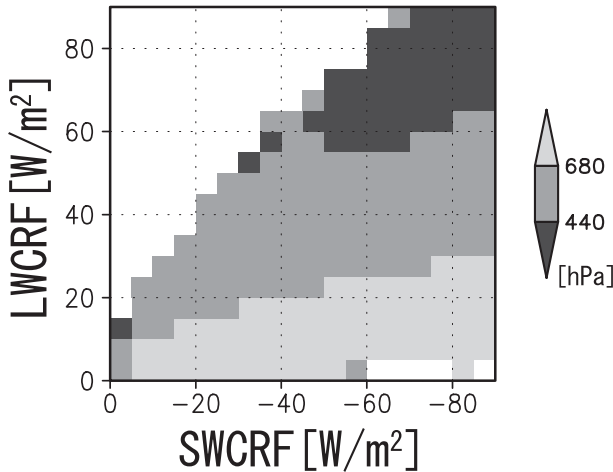
FIG. 6. Mean cloud-top pressure for each magnitude of LWCRF and SWCRF over all of the tropical oceans from the ISCCP observations.
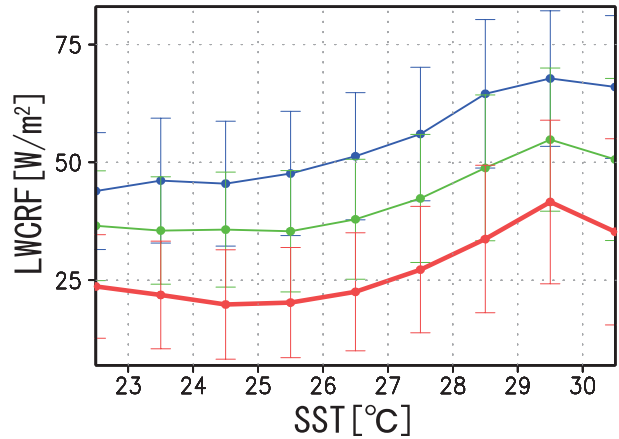
FIG. 7. Composite LWCRF as a function of SST over the strong ascent regime (blue line), the moderate ascent regime (green line), and the weak vertical motion regime (red line) for the ERBE observations. Vertical bars represent ±1 standard deviation around the mean at each SST.

4) RELATIONSHIP OF SWCRF WITH CLOUD AMOUNT

In Fig. 3b, the absolute value of SWCRF in models in the weak vertical motion regime is overestimated. SWCRF increases with cloud amount and/or cloud reflectivity, corresponding to the cloud albedo effect. Figure 10a shows the PDF of the total cloud amount in the weak vertical motion regime for the ISCCP observations and models. The PDFs largely differ among the models. In general, the PDFs of the models tend to be biased leftward against those of the ISCCP observations, indicating that the models underestimate the total cloud amount. The models' overestimation of SWCRF (Fig. 3b) in spite of the underestimation of total cloud amount (Fig. 10a)

suggests that clouds in the models are more reflective than clouds in the observations. To confirm this result, Fig. 10b shows SWCRF as a function of total cloud amount for the ERBE observations and the models. The models overestimate SWCRF at any given value of the total cloud amount. In particular, the overestimation is large at total cloud amounts between 20% and 70% where the PDFs are high in most models.

5. Discussion

a. Reproducibility of high-cloud amount

In section 4, we found that LWCRF is underestimated for the weak vertical motion regime with high SSTs in
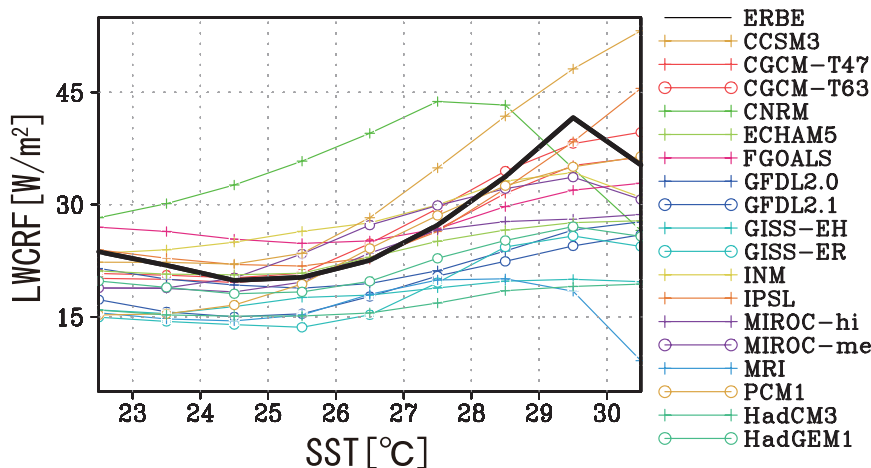
FIG. 8. Composite LWCRF as a function of SST over the weak vertical motion regime for the ERBE observations (black solid line) and the 18 models (colored solid lines).
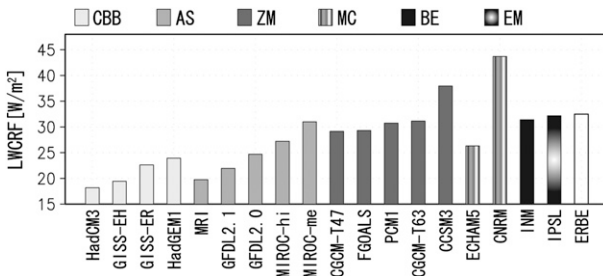
FIG. 9. Mean LWCRF over the weak vertical motion regime within the domain of SSTs above 27°C for the ERBE observations (nonshaded bar) and the 18 models (shaded bar). Models are classified by cumulus parameterization scheme (see text for details).

most models. Observational evidence showed that, in this regime, deep convection is occasionally activated while shallow convection is generally more favored (e.g., Takayabu et al. 2010). The lower free troposphere (around 600–800 hPa) in this regime seems to be dry in different reanalysis datasets [Fig. 11 in this paper and Fig. 14 in Takayabu et al. (2010)]. The dry air above the boundary layer would be unfavorable for the occurrence of deep convection (e.g., Gregory and Miller 1989; Blyth 1993; Derbyshire et al. 2004). While deep convection is only occasional, the cloud statistics in Fig. 12 indicate frequent occurrences of high clouds, in particular cirrus clouds (see Fig. 12's caption for the definition), compared to middle and low clouds in this regime. Extensive anvil clouds, which accompany deep convection, are suggested to prevail. Cirrus clouds formed away from deep convection have also been known to exist from observations (e.g., Comstock and Jakob 2004; Luo and Rossow 2004).

The results from Figs. 5 and 6 suggest that the observed high-cloud amount seems to be underestimated in the models, resulting in the underestimation of LWCRF in the models. In this section, we actually analyze the model reproducibility of the high-cloud amount in the ISCCP observations. Figure 13 shows the high-cloud amount as

a function of $\omega 500$ for the observations and for the 16 of the 18 models where the cloud amount is available for multiple vertical layers. It is noted that, for the weak vertical motion regime, the high-cloud amount is underestimated for most models. Because of the intrinsic inconsistency in the definition of cloudiness between the observations and models, it is quite difficult to properly define the cloud amount in a model. Although this point should be kept in mind, when we consider the strong impacts of high clouds on LWCRF (e.g., Hartmann et al. 2001; Kubar et al. 2007), our results possibly suggest that the models underestimate the high-cloud amount and thus underestimate LWCRF in the weak vertical motion regime.

Two models of MIROC-hi and MIROC-me overestimate the high-cloud amount in the whole regime (Fig. 13) while these models underestimate LWCRF (Fig. 3a) in the weak vertical motion regime. In the two models, the high-cloud amount identified by the current maximum overlap assumption method exceeds the total cloud amount, which is available in CMIP3 model outputs for different regimes of $\omega 500$ with high SSTs. The high-cloud amount is likely overestimated in the two models as was pointed out by Karlsson et al. (2008) and Ichikawa et al. (2009). An ongoing analysis by the authors using ISCCP simulator outputs from slab-ocean experiments in the Cloud Feedback Model Intercomparison Project (CFMIP) indicates that one of the two versions of MIROC, which is identical to MIROC-me, simulates a large amount of clouds with an optical thickness of less than 0.3. The model does not overestimate the high-cloud amount compared to the observations when clouds with optical thicknesses of less than 0.3, which are thought to be a detectable limit of the ISCCP observations, are omitted.

b. The impacts of the physical parameterizations

We have seen that LWCRF biases are somewhat related to cumulus parameterization schemes adopted in
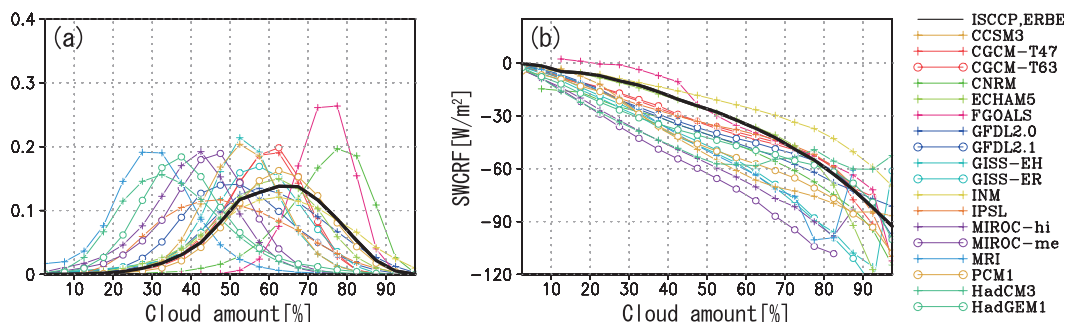
FIG. 10. (a) PDF of total cloud amount and (b) composite of SWCRF as a function of total cloud amount binned every 5% in the weak vertical motion regime within the domain of SSTs above 27°C for the ISCCP and ERBE observations (black solid line) and the 18 models (colored solid lines).
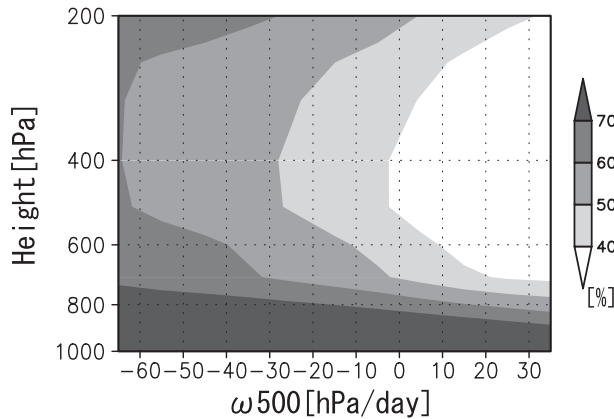
FIG. 11. Composite of the vertical distribution of the relative humidity as a function of $\omega 500$ within the domain of SSTs above 27°C for ERA-40.

FIG. 12. Cloud amount (%) for nine types of clouds based on the ISCCP D2 estimate over the weak vertical motion regime within the domain of SSTs above 27°C. In the ISCCP classification, the detected cloud-top pressure is lower than 440 hPa for high clouds, between 680 and 440 hPa for middle clouds, and higher than 680 hPa for low clouds. High clouds with optical thicknesses less than 3.6 are referred to as cirrus clouds in the text.

models. The reproducibility of LWCRF is high in the two models adopting the BE and EM schemes. The relative frequency of occurrence of the magnitudes of LWCRF (Fig. 5), as well as the mean value (Fig. 9) in the two models, are quite close to the observations. In addition to the models adopting the two schemes, the reproducibility is generally high in the models adopting the ZM scheme, as judged from the mean value (Fig. 9). The reproducibility tends to also be high in the models using the AS scheme with a relative humidity threshold.

In the BE, EM, and AS schemes with a relative humidity threshold, the relative humidity–based suppression mechanism is implemented for the occurrence of deep convection (see section 2b for details). The relative humidity–based suppression may effectively accumulate moisture at low levels of the atmosphere (from the

surface to the lower free troposphere) by suppressing excessive convection that ventilates the lower atmosphere too quickly. The accumulation of moisture at the low levels of the atmosphere would eventually be favorable for the occurrence of vigorous deep convection. The humidity-based suppression, on the other hand, is not necessarily critical for other cumulus parameterization schemes. In the case of the ZM scheme, a certain minimum depth of convection is intrinsically ensured (see section 2b for details). This assumption may be favorable for the occurrence of deep convection. Previous studies showed that the ZM scheme tends to produce dry biases in the
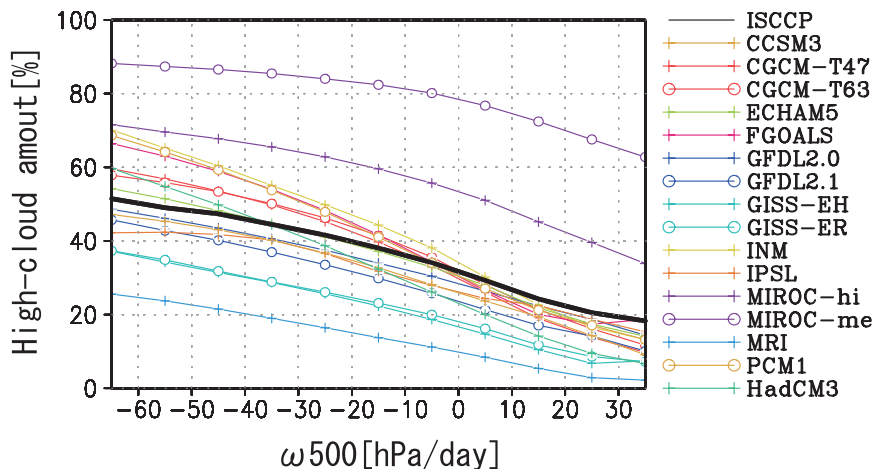
FIG. 13. Composite high-cloud amount as a function of $\omega 500$ within the domain of SSTs above 27°C for the ISCCP observations (black solid line) and the 16 available models (colored solid lines).
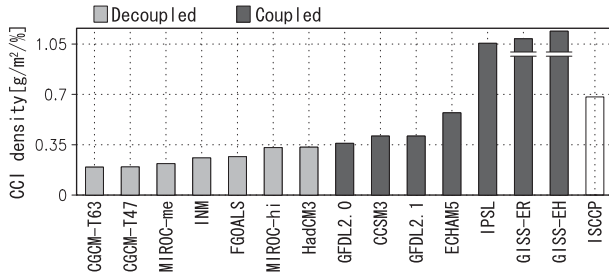
FIG. 14. Mean column-integrated CCI normalized by high-cloud amount over the weak vertical motion regime within the domain of SSTs above 27°C for the ISCCP D2 estimate (nonshaded bar) and the 14 available models (shaded bar). Models are classified by the coupling–decoupling of the cumulus parameterization scheme and the large-scale condensation scheme (see text for details). For GISS-EH and GISS-ER, the value is divided by 4.0.

FIG. 15. Composite of R as a function of $\omega 500$ for different reanalyses (solid line, ERA-40; solid line with closed circles, JRA-25; solid line with open circles, R-2) within the domain of SSTs above 27°C for the ERBE observations and the model mean for the 18 models (dashed line).

lower troposphere, probably through frequent convection (Zhang et al. 1998; xie and Zhang 2000; Zhang 2002).

Our results suggest that the parameters such as CAPE or CBB alone are not necessarily responsible for suitably reproducing deep convection over the weak vertical motion regime with high SSTs where the lower free troposphere is dry. It is supposed that, unless a suitable suppression mechanism is imposed to promote deep convection occurrence in the models, convection is forced to occur in rapid response to heat flux from a warm sea surface without sufficiently accumulating moisture at low levels of the atmosphere. Thus, convection would be less vigorous than expected for models without a realistic suppression mechanism incorporated. This may support Derbyshire et al. (2004), who showed that the upward mass flux of parameterized deep convection in the middle to upper levels of the atmosphere is weaker in the scheme where the occurrence of deep convection is insensitive to the free-tropospheric relative humidity than in the same scheme with large sensitivity.

The reproducibility of high-cloud amount is roughly similar to that of LWCRF and depends on the cumulus parameterization scheme (not shown). A detailed evaluation of the deep convection and associated clouds in the models involves an analysis of the condensed cloud ice (CCI) content as well as the high-cloud amount. To approximate the CCI density within individual cloud cells, the CCI content normalized by the high-cloud amount is examined for the weak vertical motion regime (Fig. 14). The ISCCP estimates of the cloud ice path obtained from the combination of the observed optical thickness with the prescribed particle size distribution are used for the plot in Fig. 14. The model reproducibility of the CCI content is assessed in terms of two types of models, as described in section 2b. The reproduced tendency of the CCI content varies between the two types of models. In general, the CCI content is
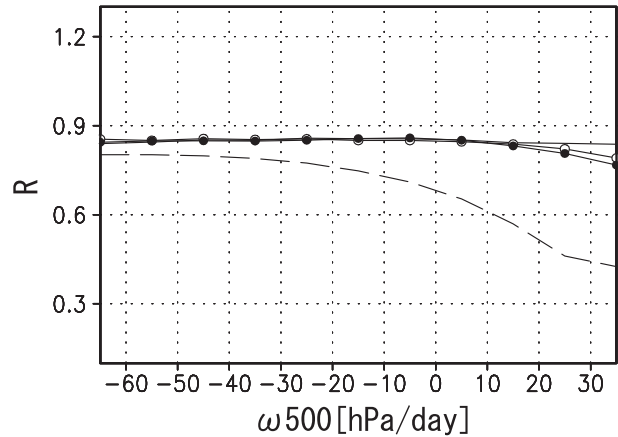
higher in the coupled models than that in the decoupled models. The difference in the CCI content among the coupled models is larger than that among the decoupled models. Further evaluations of cloud microphysics would involve an analysis of the vertical distribution of CCI, but are beyond the scope of this paper.

c. Consistency of results among different observational and reanalysis datasets

In the analyses described above, $\omega 500$s of ERA-40 are used to evaluate model outputs. Vertical velocity fields may differ among reanalysis datasets. Thus, the results obtained from the analyses using ERA-40 need to be compared with those using other reanalysis datasets. The same analyses conducted with ERA-40 are performed with data from the Japanese 25-yr Reanalysis (JRA-25; Onogi et al. 2007) and the National Centers for Environmental Prediction–Department of Energy (NCEP–DOE) Atmospheric Model Intercomparison Project II (AMIP-II) reanalysis (R-2; Kanamitsu et al. 2002). It is confirmed that the results are consistent among the three reanalysis datasets. Figure 15 shows that systematic underestimation of R in the models at the weak vertical motion regime compared to the ERBE observations is seen in all three different reanalysis datasets. We also confirmed that the results are generally consistent in all other aspects of the analyses in the present study among three reanalysis datasets.

We further compare the results using the ERBE observation for 5 yr and 1 month from February 1985 to February 1990 with those using the Clouds and Earth's Radiant Energy System (CERES) observations (Smith et al. 2004) for 6 yr from 2000 to 2005. The simulations

also produce unrealistically low values of R when compared to CERES observations (not shown). The absolute values of LWCRF and SWCRF in the CERES observations are smaller than those in the ERBE observation for different regimes of $\omega 500$ while the difference is not so large as to undermine the results of this study.

6. Concluding remarks

This study evaluates the CRF associated with convective activity over tropical oceans for the 18 climate models participating in the CMIP3. CRF is evaluated for different regimes of the large-scale circulation field sorted by $\omega 500$ to consider the effects of large-scale circulation on CRF in the models. Over warm oceanic regions with SSTs above 27°C where convection is active, LWCRF and SWCRF in the ERBE observations nearly cancel each other independently of different regimes of large-scale circulation. We intensively evaluate the model reproducibility of the ERBE observations, focusing on the warm oceanic regions. The warm oceanic regions cover the regime of $\omega 500$ ranging from strong ascent to weak descent. A notable systematic bias can be found in the weak vertical motion regime defined as $-10 < \omega 500 < 20$ hPa day^{-1}: R, the absolute value of the ratio of LWCRF to SWCRF, is underestimated in most of the models compared to the ERBE observations. The weak vertical motion regime contributes to roughly 35% of occurrence in the domain of the warm SSTs. The bias of R is attributed to the underestimation of LWCRF and the overestimation of SWCRF in the absolute value. The models tend to underestimate high clouds but overestimate cloud reflectivity for a given cloud amount.

The lower free troposphere over the weak vertical motion regime with high SSTs is dry. The dryness is unfavorable for the occurrence of deep convection, which is considered to be sensitive to the relative humidity in the free troposphere (e.g., Gregory and Miller 1989; Blyth 1993; Derbyshire et al. 2004). Under large-scale environment conditions, deep convection occasionally occurs in this regime (e.g., Takayabu et al. 2010) presumably through the reduction of the dryness due to the moisture development in low levels of the atmosphere in some periods. The model reproducibility of LWCRF, which is affected by deep convection, over this regime reflects the sensitivity of deep convection occurrences to relative humidity in the free troposphere in cumulus parameterization schemes adopted in each model. The reproducibility is high in the schemes where the relative humidity–based suppression mechanism is implemented for the occurrence of deep convection [Arakawa–Schubert-type scheme with a threshold proposed by Emori et al. (2001), Betts scheme, Emanuel scheme with a modification proposed by Grandpeix et al. (2004)], while the Zhang and McFarlane scheme shows good performance without such a suppression mechanism. The relative humidity–based suppression may effectively accumulate moisture at low levels of the atmosphere. Our results are consistent with previous studies that indicated the importance of convection suppression for the proper representation of deep convection (e.g., Emori et al. 2001; Zhang 2002; Grandpeix et al. 2004; Hirota et al. 2011).

Further analyses would be needed to fully unravel the model physics responsible for the model bias of CRF revealed in this study. The analyses would involve the evaluation of cloud properties. The method adopted in this study would be one of the useful approaches to evaluating the model reproducibility of CRF associated with the convective activity, and can be used to evaluate it in model simulations for the IPCC's Fifth Assessment Report (AR5).

REFERENCES

Arakawa, A., and W. H. Schubert, 1974: Interaction of a cumulus cloud ensemble with the large-scale environment, Part I. *J. Atmos. Sci.,* **31,** 674–701.

Baldwin, M. E., J. S. Kain, and M. P. Kay, 2002: Properties of the convection scheme in NCEP's Eta Model that affect forest sounding interpretation. *Wea. Forecasting,* **17,** 1063–1079.

Barkstrom, B. R., 1984: The Earth Radiation Budget Experiment (ERBE). *Bull. Amer. Meteor. Soc.,* **65,** 1170–1185.

——, and G. L. Smith, 1986: The Earth Radiation Budget Experiment: Science and implementation. *Rev. Geophys.,* **24,** 379–390.

Betts, A. K., 1986: New convective adjustment scheme, Part 1. Observational and theoretical basis. *Quart. J. Roy. Meteor. Soc.,* **112,** 677–691.

Blyth, A. M., 1993: Entrainment in cumulus clouds. *J. Appl. Meteor.,* **32,** 626–641.

Bony, S., and K. A. Emmanuel, 2001: A parameterization of the cloudiness associated with cumulus convection: Evaluation using TOGA COARE data. *J. Atmos. Sci.,* **58,** 3158–3183.

——, K.-M. Lau, and Y. C. Sud, 1997: Sea surface temperature and large-scale circulation influences on tropical greenhouse effect and cloud radiative forcing. *J. Climate,* **10,** 2055–2077.

——, J.-L. Dufresne, H. L. Treut, J.-J. Morcrette, and C. Senior, 2004: On dynamic and thermodynamic components of cloud changes. *Climate Dyn.,* **22,** 71–86.

Bougeault, P., 1985: A simple parameterization of the large-scale effects of cumulus convection. *Mon. Wea. Rev.,* **113,** 2108–2121.

Cess, R. D., M. Zhang, B. A. Wielicki, D. F. Young, X.-L. Zhou, and Y. Nikitenko, 2001: The influence of the 1998 El Niño upon cloud radiative forcing over the Pacific warm pool. *J. Climate,* **14,** 2129–2137.

Charlock, T., and V. Ramanathan, 1985: The albedo field and cloud radiative forcing in a general circulation model with internally generated cloud optics. *J. Atmos. Sci.,* **42,** 1408–1429.

Comstock, J. M., and C. Jakob, 2004: Evaluation of tropical cirrus cloud properties derived from ECMWF model output and ground based measurements over Nauru Island. *Geophys. Res. Lett.,* **31,** L10106, doi:10.1029/2004GL019539.

Dai, A., 2006: Precipitation characteristics in 18 coupled climate models. *J. Climate,* **19,** 4605–4630.

Del Genio, A. D., and M.-S. Yao, 1993: Efficient cumulus parameterization for long-term climate studies: The GISS scheme. *The Representation of Cumulus Convection in Numerical Models, Meteor. Monogr.,* No. 46, Amer. Meteor. Soc., 181–184.

——, ——, ——, W. Kovari, and K. K. W. Lo, 1996: A prognostic cloud water parameterization for global climate models. *J. Climate,* **9,** 270–304.

——, W. Kovari, M.-S. Yao, and J. Jonas, 2005: Cumulus microphysics and climate sensitivity. *J. Climate,* **18,** 2376–2387.

Derbyshire, S. H., I. Beau, P. Bechtold, J.-Y. Grandpeix, J.-M. Piriou, J.-L. Redelsperger, and P. M. M. Soares, 2004: Sensitivity of moist convection to environmental humidity. *Quart. J. Roy. Meteor. Soc.,* **130,** 3055–3079.

Diansky, N. A., and E. M. Volodin, 2002: Simulation of present-day climate with a coupled atmosphere–ocean general circulation model. *Izv., Atmos. Oceanic Phys.,* **38,** 732–747.

Emanuel, K. A., 1991: A scheme for representing cumulus convection in large-scale models. *J. Atmos. Sci.,* **48,** 2313–2329.

Emori, S., T. Nozawa, A. Numaguti, and I. Uno, 2001: Importance of cumulus parameterization for precipitation simulation over East Asia in June. *J. Meteor. Soc. Japan,* **79,** 939–947.

Gadgil, S., P. V. Joseph, and N. V. Joshi, 1984: Ocean–atmospheric coupling over monsoon regions. *Nature,* **312,** 141–143.

Graham, N., and T. P. Barnett, 1987: Sea surface temperature, surface wind divergence, and convection over tropical oceans. *Science,* **238,** 657–659.

Grandpeix, J. Y., V. Phillips, and R. Tailleux, 2004: Improved mixing representation in Emanuel's convection scheme. *Quart. J. Roy. Meteor. Soc.,* **130,** 3207–3222.

Gregory, D., and M. J. Miller, 1989: A numerical study of the parameterization of deep tropical convection. *Quart. J. Roy. Meteor. Soc.,* **115,** 1209–1241.

——, and P. R. Rowntree, 1990: A mass flux convection scheme with representation of cloud ensemble characteristics and stability-dependent closure. *Mon. Wea. Rev.,* **118,** 1483–1506.

Hartmann, D. L., and D. Doelling, 1991: On the net radiative effectiveness of clouds. *J. Geophys. Res.,* **96,** 869–891.

——, and M. L. Michelsen, 1993: Large-scale effects on the regulation of tropical sea surface temperature. *J. Climate,* **6,** 2049–2062.

——, L. A. Moy, and Q. Fu, 2001: Tropical convection and the energy balance at the top of the atmosphere. *J. Climate,* **14,** 4495–4511.

Hirota, N., Y. N. Takayabu, M. Watanabe, and M. Kimoto, 2011: Precipitation reproducibility over tropical oceans and its relationship to the double ITCZ problem in CMIP3 and MIROC5 climate models. *J. Climate,* **24,** 4859–4873.

Ichikawa, H., H. Masunaga, and H. Kanzawa, 2009: Evaluation of precipitation and high-level cloud areas associated with large-scale circulation over the tropical Pacific in the CMIP3 models. *J. Meteor. Soc. Japan,* **87,** 771–789.

Kanamitsu, M., W. Ebisuzaki, J. Woollen, S.-K. Yang, J. J. Hnilo, M. Fiorino, and G. L. Potter, 2002: NCEP–DOE AMIP-II Reanalysis (R-2). *Bull. Amer. Meteor. Soc.,* **83,** 1631–1643.

Karlsson, J., G. Svensson, and H. Rodhe, 2008: Cloud radiative forcing of subtropical low level clouds in global models. *Climate Dyn.,* **30,** 779–788.

Kiehl, J. T., 1994: On the observed near cancellation between longwave and shortwave cloud forcing in tropical regions. *J. Climate,* **7,** 559–565.

——, and V. Ramanathan, 1990: Comparison of cloud forcing derived from the Earth Radiation Budget Experiment with that simulated by the NCAR Community Climate Model. *J. Geophys. Res.,* **95,** 11 679–11 698.

Klein, S., and C. Jakob, 1999: Validation and sensitivities of frontal clouds simulated by the ECMWF model. *Mon. Wea. Rev.,* **127,** 2514–2531.

Kosaka, Y., H. Nakamura, M. Watanabe, and M. Kimoto, 2009: Analysis of the dynamics of a wave-like teleconnection pattern along the summertime Asian jet based on a reanalysis dataset and climate model simulations. *J. Meteor. Soc. Japan,* **87,** 561–580.

Kubar, T. L., D. L. Hartmann, and R. Wood, 2007: Radiative and convective driving of tropical high clouds. *J. Climate,* **20,** 5510–5527.

Kuo, H. L., 1965: On formation and intensification of tropical cyclones through latent heat release by cumulus convection. *J. Atmos. Sci.,* **22,** 40–63.

Lau, K.-M., H.-T. Wu, and S. Bony, 1997: The role of large-scale atmospheric circulation in the relationship between tropical convection and sea surface temperature. *J. Climate,* **10,** 381–392.

Le Trent, H., and Z.-X. Li, 1991: Sensitivity of an atmospheric general circulation model to prescribed SST changes: Feedback effects associated with the simulation of cloud optical properties. *Climate Dyn.,* **5,** 175–187.

Lin, J.-L., 2007: The double-ITCZ problem in IPCC AR4 coupled GCMs: Ocean–atmosphere feedback analysis. *J. Climate,* **20,** 4497–4525.

Lindzen, R. S., M.-D. Chou, and A. Y. Hou, 2001: Does the earth have an adaptive infrared iris? *Bull. Amer. Meteor. Soc.,* **82,** 417–432.

Lohmann, U., and E. Roeckner, 1996: Design and performance of a new cloud microphysics parameterization developed for the ECHAM4 general circulation model. *Climate Dyn.,* **12,** 557–572.

Luo, Z., and W. B. Rossow, 2004: Characterizing tropical cirrus life cycle, evolution, and interaction with upper-tropospheric water vapor using Lagrangian trajectory analysis of satellite observations. *J. Climate,* **17,** 4541–4563.

Masunaga, H., and C. D. Kummerow, 2006: Observations of tropical precipitating clouds ranging from shallow to deep convective systems. *Geophys. Res. Lett.,* **33,** L16805, doi:10.1029/2006GL026547.

McFarlane, N. A., J. F. Scinocca, M. Lazare, R. Harvey, D. Verseghy, and J. Li, 2005: The CCCma third generation

atmospheric general circulation model. CCCma Internal Rep., 25 pp.

Moorthi, S., and M. J. Suarez, 1992: Relaxed Arakawa-Schubert: A parameterization of moist convection for general circulation models. *Mon. Wea. Rev.,* **120,** 978–1002.

Nordeng, T. E., 1994: Extended versions of the convective parameterization scheme at ECMWF and their impact on the mean and transient activity of the model in the tropics. ECMWF Tech. Memo. 206, 41 pp.

Onogi, K., and Coauthors, 2007: The JRA-25 Reanalysis. *J. Meteor. Soc. Japan,* **85,** 369–432.

Pan, D.-M., and D. A. Randall, 1998: A cumulus parameterization with a prognostic closure. *Quart. J. Roy. Meteor. Soc.,* **124,** 949–981.

Ramanathan, V., and W. Collins, 1991: Thermodynamic regulation of ocean warming by cirrus clouds deduced from observations of the 1987 El Niño. *Nature,* **351,** 27–32.

——, R. D. Cess, E. F. Harrison, P. Minnis, B. R. Barkstrom, and D. L. Hartmann, 1989: Cloud-radiative forcing and climate: Results from the Earth Radiation Budget Experiment. *Science,* **243,** 57–63.

Rasch, P., and J. E. Kristjansson, 1998: A comparison of the CCM3 model climate using diagnostic and predicted condensate parameterizations. *J. Climate,* **11,** 1587–1614.

Rayner, N. A., D. E. Parker, E. B. Horton, C. K. Folland, L. V. Alexander, D. P. Rowell, E. C. Kent, and A. Kaplan, 2003: Global analysis of sea surface temperature, sea ice, and night marine air temperature since the late nineteenth century. *J. Geophys. Res.,* **108,** 4407, doi:10.1029/2002JD002670.

Ricard, J. L., and J. F. Royer, 1993: A statistical cloud scheme for use in an AGCM. *Ann. Geophys. Atmos. Space Sci.,* **11,** 1095–1115.

Rossow, W. B., and R. A. Schiffer, 1999: Advances in understanding clouds from ISCCP. *Bull. Amer. Meteor. Soc.,* **80,** 2261–2287.

Smith, G. L., and Coauthors, 2004: Clouds and Earth Radiant Energy System: An overview. *Adv. Space Res.,* **33,** 1125–1131.

Smith, R. N. B., 1990: A scheme for predicting layer clouds and their water content in a general circulation model. *Quart. J. Roy. Meteor. Soc.,* **116,** 435–460.

Solomon, S., D. Qin, M. Manning, M. Marquis, K. Averyt, M. M. B. Tignor, H. L. Miller Jr., and Z. Chen, Eds., 2007: *Climate Change 2007: The Physical Science Basis.* Cambridge University Press, 996 pp.

Su, H., D. E. Waliser, J. H. Jiang, J.-L. Li, W. G. Read, J. W. Waters, and A. M. Tompkins, 2006: Relationship of upper tropospheric water vapor, clouds and SST: MLS observations, ECMWF analyses and GCM simulations. *Geophys. Res. Lett.,* **33,** L22802, doi:10.1029/2006GL027582.

Takayabu, Y. N., S. Shige, W.-K. Tao, and N. Hirota, 2010: Shallow and deep latent heating modes over tropical oceans observed with TRMM PR spectral latent heating data. *J. Climate,* **23,** 2030–2046.

Tiedtke, M., 1989: A comprehensive mass flux scheme for cumulus parameterization in large-scale models. *Mon. Wea. Rev.,* **117,** 1779–1800.

——, 1993: Representation of clouds in large-scale models. *Mon. Wea. Rev.,* **121,** 3040–3061.

Tokioka, T., K. Yamazaki, A. Kitoh, and T. Ose, 1988: The equatorial 30–60 day oscillation and the Arakawa–Schubert penetrative cumulus parameterization. *J. Meteor. Soc. Japan,* **66,** 883–901.

Uppala, S. M., and Coauthors, 2005: The ERA-40 Re-Analysis. *Quart. J. Roy. Meteor. Soc.,* **131,** 2961–3012.

Weare, B. C., 2004: A comparison of AMIP II model cloud layer properties with ISCCP D2 estimates. *Climate Dyn.,* **22,** 281–292.

Webb, M., C. Senior, S. Bony, and J.-J. Morcrette, 2001: Combining ERBE and ISCCP data to assess clouds in the Hadley Centre, ECMWF, and LMD atmospheric models. *Climate Dyn.,* **17,** 905–922.

Williams, K. D., and G. Tselioudis, 2007: GCM intercomparison of global cloud regime: Present-day evaluation and climate change response. *Climate Dyn.,* **29,** 231–250.

——, and M. Webb, 2009: A quantitative performance assessment of cloud regimes in climate models. *Climate Dyn.,* **33,** 141–157.

——, M. A. Ringer, and C. A. Senior, 2003: Evaluating the cloud response to climate change and current climate variability. *Climate Dyn.,* **20,** 705–721.

Wilson, D. R., and S. P. Ballard, 1999: A microphysically based precipitation scheme for the UK Meteorological Office Unified Model. *Quart. J. Roy. Meteor. Soc.,* **125,** 1607–1636.

Wyant, M. C., C. S. Bretherton, J. T. Kiehl, I. M. Held, M. Z. Zhao, S. A. Klein, and B. J. Soden, 2006: A comparison of tropical cloud properties and responses in GCMs using midtropospheric vertical velocity. *Climate Dyn.,* **27,** 261–279.

Xie, S., and M. Zhang, 2000: Impact of the convective triggering function on single-column model simulations. *J. Geophys. Res.,* **105,** 14 983–14 996.

Yuan, J., D. L. Hartmann, and R. Wood, 2008: Dynamic effects on the tropical cloud radiative forcing and radiation budget. *J. Climate,* **21,** 2337–2351.

Yukimoto, S., and Coauthors, 2006: Present-day climate and climate sensitivity in the Meteorological Research Institute Coupled GCM, version 2.3 (MRI-CGCM2.3). *J. Meteor. Soc. Japan,* **84,** 333–363.

Zhang, G. J., 2002: Convective quasi-equilibrium in midlatitude continental environment and its effect on convective parameterization. *J. Geophys. Res.,* **107,** 4220, doi:10.1029/2001JD001005.

——, and N. A. McFarlane, 1995: Sensitivity of climate simulations to the parameterization of cumulus convection in the CCC-GCM. *Atmos.–Ocean,* **3,** 407–446.

——, J. T. Kiehl, and P. J. Rasch, 1998: Response of climate simulation to a new convective parameterization in the National Center for Atmospheric Research Community Climate Model (CCM3). *J. Climate,* **11,** 2097–2115.

Zhang, M., W. Lin, C. B. Bretherton, J. J. Hack, and P. J. Rasch, 2003: A modified formulation of fractional stratiform condensation rate in the NCAR Community Atmospheric Model (CAM2). *J. Geophys. Res.,* **108,** 4035, doi:10.1029/2002JD002523.